




Measurement of interdiffusion and impurity diffusion coefficients in the bcc phase of the Ti–X (X = Cr, Hf, Mo, Nb, V, Zr) binary systems using diffusion multiples

Lilong Zhu^{1,2}, Qiaofu Zhang³, Zhangqi Chen³, Changdong Wei³, Ge-Mei Cai^{1,*} , Liang Jiang², Zhanpeng Jin¹, and Ji-Cheng Zhao^{3,*}

¹ School of Materials Science and Engineering, Central South University, Changsha 410083, Hunan, People's Republic of China

² State Key Laboratory of Powder Metallurgy, Central South University, Changsha 410083, Hunan, People's Republic of China

³ Department of Materials Science and Engineering, The Ohio State University, Columbus OH, 43210, USA

Received: 18 August 2016

Accepted: 17 November 2016

Published online:

28 November 2016

© Springer Science+Business Media New York 2016

ABSTRACT

The design and development of novel titanium alloys for structural and biomedical applications require reliable thermodynamic and kinetic databases. In this study, diffusion behaviors of six Ti–X (X = Cr, Hf, Mo, Nb, V, Zr) binary systems were systematically investigated at temperatures from 800 to 1200 °C using a set of five Ti–TiAl–Cr–Hf–Mo–Nb–V–Zr diffusion multiples. Concentration profiles of the six Ti–X binary systems were collected from binary regions of the diffusion multiples using electron probe microanalysis (EPMA). Both interdiffusion and impurity (dilute) diffusion coefficients in the Ti-rich bcc phase of these systems were extracted from the concentration profiles using the forward-simulation method. Twenty impurity diffusion coefficients of all the six elements in bcc Ti as well as Ti in bcc Zr at different temperatures obtained from this study are in excellent agreement with the literature data. The interdiffusion coefficients obtained from this study are also in good agreement with previous literature results. The large amount of new experimental data obtained from this study will be essential for establishing the mobility databases for the design and development of advanced titanium alloys.

Introduction

Titanium and its alloys have been extensively used in the aerospace industry because of the combination of properties including the high specific strength (strength-to-density ratio), excellent corrosion resistance, and high-temperature stability [1, 2]. Ti alloys have also been

attracting significant attention for biomedical applications due to their good biocompatibility, high corrosion resistance, and low elastic modulus as compared to other metallic biomaterials [3, 4].

Pure Ti and most Ti alloys exhibit an allotropic phase transformation between the low-temperature α (hcp) phase and the high-temperature β (bcc) phase.

Address correspondence to E-mail: caigemei@csu.edu.cn; zhao.199@osu.edu

Table 1 Summary of the interdiffusion coefficients of the Ti–X (X = Cr, Mo, Nb, V, Hf, Zr) binary systems reported in literature [14–32]

System	Diffusion Couples (alloy composition in at.%)	Temperature range (°C)	Methods for diffusivity extraction	References
Ti–Cr	Ti/Ti–4.62Cr	900–1550	Boltzmann–Matano	Lee et al. [14]
	Ti–5Cr/Ti–15Cr	898–1299	Boltzmann–Matano	Sprengel et al. [15]
	Ti/Ti–4.8Cr, Ti/Ti–14.4Cr	1100–1200	Boltzmann–Matano	Takahashi et al. [16]
Ti–Mo	Ti–5Mo/Ti–15Mo	851–1299	Boltzmann–Matano	Sprengel et al. [15]
	Ti/Mo, Ti/Ti–50Mo, Mo/Ti–50Mo	820–1600	Boltzmann–Matano	Hartley et al. [17]
	Ti/Mo, Ti/Ti–27Mo	900–1500	Boltzmann–Matano	Fedotov et al. [18]
	Ti/Mo	1027–1527	Boltzmann–Matano	Heumann and Imm [19]
	Ti/Mo	1200–1400	Boltzmann–Matano	Majima and Isomoto [20]
	Ti/Mo	926–1245	Boltzmann–Matano	Kale and Patil [21]
	Ti/Mo, Ti–25.6Mo, Ti–33.9Mo	1250–1800	Den Broeder	Thibon et al. [22]
	Ti/Mo	950–1050	Den Broeder	Feng et al. [23]
Ti–Nb	Ti/Nb, Ti/Ti–50Nb, Nb/Ti–50Nb	1000–1588	Boltzmann–Matano	Hartley et al. [17]
	Ti/Nb, Nb/Ti–44Nb	900–1350	Boltzmann–Matano	Fedotov et al. [18]
	Ti/Nb, Nb/Ti–Nb alloys	1450–2075	Boltzmann–Matano and Hall	Roux and Vignes [24]
	Ti/Nb	1000–1200	Boltzmann–Matano	Polyanskii et al. [25]
	Ti/Nb	800–1200	Boltzmann–Matano	Gryzunov et al. [26]
Ti–V	Ti–5V/Ti–15V	895–1136	Boltzmann–Matano	Sprengel et al. [15]
	Ti/V, V/Ti–44.5V	900–1500	Boltzmann–Matano	Fedotov et al. [18]
	Ti/V	1000–1400	Boltzmann–Matano	Ugaste and Zaykin [27]
	Ti–Hf	1000–2000	Den Broeder	Gall et al. [28]
Ti–Zr	Zr/Ti–(12, 18, 34, 55, 68) Zr	901–1168	Boltzmann–Matano	Raghunathan et al. [29]
	Ti/Zr	650–1050	Boltzmann–Matano	Brunsch and Steeb [30]
	Ti/Zr, Ti/Ti–Zr alloys	900	Boltzmann–Matano and Hall	Bhanumurthy et al. [31]
	Ti/Zr, Ti/Ti–5Zr, Ti–85Zr/Ti–15Zr, Zr/Ti–64Zr	830–1730	Den Broeder	Thibon et al. [32]

The existence of the two different crystal structures as well as the corresponding α to β transus temperature (known as β -transus) are the bases for a large variety of properties achieved by Ti alloys. Compared to α and $\alpha + \beta$ alloys, β Ti alloys have superior fatigue resistance as well as wear and abrasion resistance, which makes β Ti alloys highly desirable for biomedical applications [5, 6]. Alloying elements such as Cr, Mo, Nb, Ta, and V serve as β -phase stabilizers, which depress the β -transus temperature and lower the elastic modulus. However, the Ti alloys developed so far still have relatively higher Young's modulus than that of human bones (20–30 GPa). Theoretical investigations by Song et al. [7] suggested that Mo, Nb, Ta, and Zr are the most desirable alloying elements in β -type bio-Ti alloys to potentially decrease the modulus and enhance the strength of the alloys. Another point worth noting is that these elements are all non-toxic, and thus ideal for biomedical applications. Hf is in the same group as Ti in the periodic table and they have complete

mutual solubility in both the α and β phases, which makes Hf another good candidate alloying element for a lower modulus. For instance, Wang et al. [8] studied the in vitro cytotoxicity and hemocompatibility of Ti–Nb–Zr and Ti–Nb–Hf alloys, demonstrating that both Zr and Hf are non-toxic and Ti–Nb–Zr/Hf alloys are highly biocompatible. More recently, González et al. [9–12] developed a new β Ti alloy, Ti–25Nb–16Hf, with a low elastic modulus of 42 GPa.

Thermodynamic phase equilibria and kinetic behavior in Ti alloys are the very basic knowledge for understanding the phase stability, phase transformation, and microstructure evolution during the alloy processing such as casting and extrusion. Such information is essential for the compositional design and the process condition optimization of bio-Ti alloys. The present work intends to determine the interdiffusion and impurity diffusion coefficients of the six Ti–X (X = Cr, Hf, Mo, Nb, V, Zr) binary systems in the temperature range between 800 and

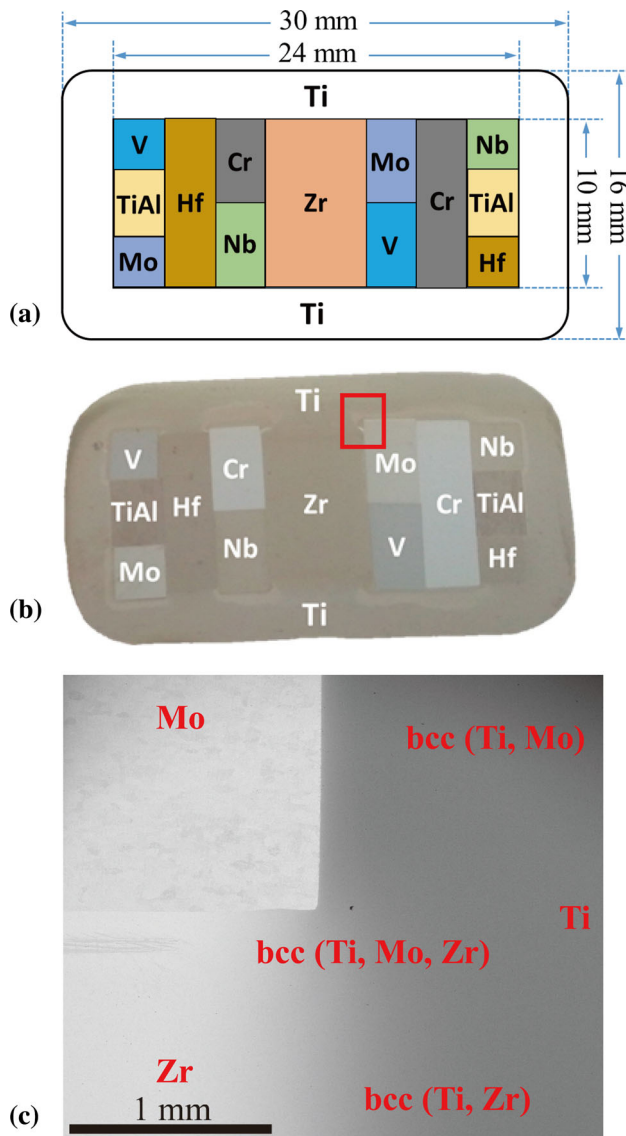


Figure 1 Images of the Ti–TiAl–Cr–Hf–Mo–Nb–V–Zr diffusion multiple: **a** cross-section view showing the dimensions of the metal pieces in the diffusion multiple; **b** a photograph of a slice of the diffusion multiple after annealing at 1100 °C for 25 h; and **c** a representative SEM BSE image taken at the location marked by a red box in **(b)** showing the phase formation after diffusion annealing.

1200 °C. The collected experimental data will help establish reliable diffusion (mobility) databases for the kinetic modeling of Ti alloys.

The self-diffusion coefficients of elements Cr, Hf, Mo, Nb, V, and Zr and their impurity diffusion coefficients in pure Ti over a wide temperature range have been well studied and reviewed by Neumann and Tuijn [13]. Interdiffusion coefficients of the Ti–Cr, Ti–Mo, Ti–Nb, Ti–V, Ti–Hf, and Ti–Zr binary systems

have also been studied by many research groups [14–32] as summarized in Table 1. EPMA was used by these groups to collect the experimental composition profiles and the diffusion coefficients were extracted using the Boltzmann–Matano method [33, 34], the Den Broeder method [35], and the Hall method [36]. Whenever possible, those literature results will be compared with the results obtained from the current study (e.g., at or close to the same temperatures) in the Results and discussion section.

Experimental procedures

A diffusion multiple [37–40] is an assembly of several pieces of metals or alloys with intimate interfacial contact in a designed geometry to contain several diffusion couples and triples in one sample, which significantly improves the efficiency of diffusion studies without the need to make many individual diffusion couples and triples. The specific geometry of a diffusion multiple depends on the eutectic temperatures (to avoid melting during diffusion annealing) and the diffusion coefficients such that the dimensions of various metal pieces should be designed to have pure elements remaining at the end of diffusion annealing. The diffusion-multiple approach has already been widely applied to the effective collection of concentration profiles by performing EPMA measurement across the diffusion regions. The measured concentration profiles could be utilized for phase diagram determination based on the local equilibrium at the phase interfaces [41], and the concentration profiles could also be used to extract composition-dependent interdiffusion coefficients at the diffusion-annealing temperatures.

Five Ti–TiAl–Cr–Hf–Mo–Nb–V–Zr diffusion multiples of identical geometry were made, as shown schematically in Fig. 1. The starting pure metals of Ti, Cr, Hf, Mo, Nb, and V have a purity of 99.99% and Zr has a purity of 99.95% (all in wt.%). The stoichiometric alloy TiAl was made by crucible-free levitation melting in an argon atmosphere and drop-casting into cold copper molds. The TiAl alloy was re-melted three times to ensure homogeneity. The ingot was then further homogenized in a vacuum furnace under a high-purity argon atmosphere at 1200 °C for 48 h, followed by furnace cooling. All the metal pieces inside the diffusion multiple were cut by electrical discharge machining (EDM) to the required dimensions, as

shown in Fig. 1a. Each diffusion multiple includes one Zr brick of dimensions $6 \times 10 \times 25$ mm, one Cr brick and one Hf brick of dimensions $3 \times 10 \times 25$ mm, one Cr, one Mo, one Nb, and one V piece of dimensions $3 \times 5 \times 25$ mm, two TiAl bars of dimensions $3 \times 4 \times 25$ mm, as well as one Hf, one Mo, one Nb, and one V plate of dimensions $3 \times 3 \times 25$ mm. A pure Ti cartridge with a 10×24 mm rectangular opening along the cylindrical axis was cut from a 35 mm diameter and 25 mm height pure Ti cylinder. The dimensions of all the metal pieces were carefully designed based on simulation/calculation of the diffusion distances between the elements using existing interdiffusion and impurity diffusion coefficient data in the literature in order to avoid the exhaustion of the pure metals and the TiAl alloy after the long-term diffusion annealing. The TiAl stoichiometric alloy was made and included in the diffusion multiple in order to determine the TiAl-based ternary phase diagrams—the results will be published separately.

After cutting, the surfaces of all the metal pieces were ground to 1200 grit SiC sand papers to get a flat surface finish. All of the pieces were ultrasonically cleaned in alcohol before being placed into the Ti cartridges. Two Ti caps of 3 mm in thickness were then electron beam welded in vacuum onto the top and bottom of each assembly. The samples then underwent a hot isostatic pressing (HIP) run at 1000 °C with an argon pressure of 310 MPa for 8 h to achieve good interfacial contact among the metal pieces. The diffusion multiples were then encapsulated individually into quartz tubes for annealing heat treatment at 1200, 1100, 1000, 900, and 800 °C for 10, 25, 120, 600, and 1100 h, respectively.

All the diffusion-multiple samples were buried in pure Ti sponges and powders during HIP and the diffusion heat treatment processes. The sponges and powders with high surface areas served as oxygen absorbers to minimize the oxidation of the samples themselves from the residual oxygen and any oxygen that diffused into the quartz tubes during the long-term annealing heat treatments. Upon completing the diffusion annealing, the samples were quenched in ice water by quickly breaking the quartz tubes inside the water tank.

The diffusion multiples were sectioned using EDM, and then mounted, ground, and polished using standard metallography sample preparation techniques. Backscattered electron (BSE) imaging in scanning electron microscopy (SEM) was employed

to analyze the phases that formed during the diffusion annealing. A representative SEM BSE image taken from the Ti–Mo–Zr tri-junction within the diffusion multiple annealed at 1100 °C for 25 h is shown in Fig. 1c, wherein the pure metals and the bcc solid solution formed by interdiffusion can be clearly identified. Composition profiles were obtained using quantitative EPMA parallel to the diffusion direction on a JEOL JXA-8530F with an accelerating voltage of 15 kV and a probe current of 20 nA. The step size and the length of each EPMA line scan were carefully chosen according to the measured line scan profiles by local energy-dispersive spectroscopy (EDS). Interdiffusion and impurity diffusion coefficients were calculated from the measured concentration profiles using the forward-simulation method [42, 43]. All the results reported in this paper came from the Ti–X (X = Cr, Hf, Mo, Nb, V, Zr) diffusion couple regions of the diffusion multiples, and results for the other systems will be obtained and reported separately.

Results and discussion

Binary phase diagrams of the six Ti–X systems were obtained from the ASM Alloy Phase Diagram Center [44], which are used to check the equilibrium composition of the solid solution and intermetallic phases. Among them, phase equilibria in the Ti–Mo, Ti–Nb, and Ti–V systems are quite similar: the bcc Ti and bcc Mo (Nb or V) are completely soluble at 900–1200 °C, while the hcp Ti begins to form at around 882 °C. Hf and Zr are in the same column as Ti in the periodic table, and these two systems share some common features: a two-phase region exists between the bcc and hcp phases, and Ti and Hf (or Zr) are completely miscible in both the bcc and hcp phases.

In the current study, the Ti–TiAl–Cr–Hf–Mo–Nb–V–Zr diffusion multiples first underwent a HIP run at 1000 °C for 8 h. During the HIP process, considerable diffusion between Ti and the other metals has already taken place before the subsequent diffusion heat treatments. As a result, the diffusion that occurred during the HIP process needs to be taken into consideration during analysis for the diffusion coefficients, and the whole diffusion simulation process was assumed to be a “two-step” process. The diffusion coefficients of all the six binary systems at

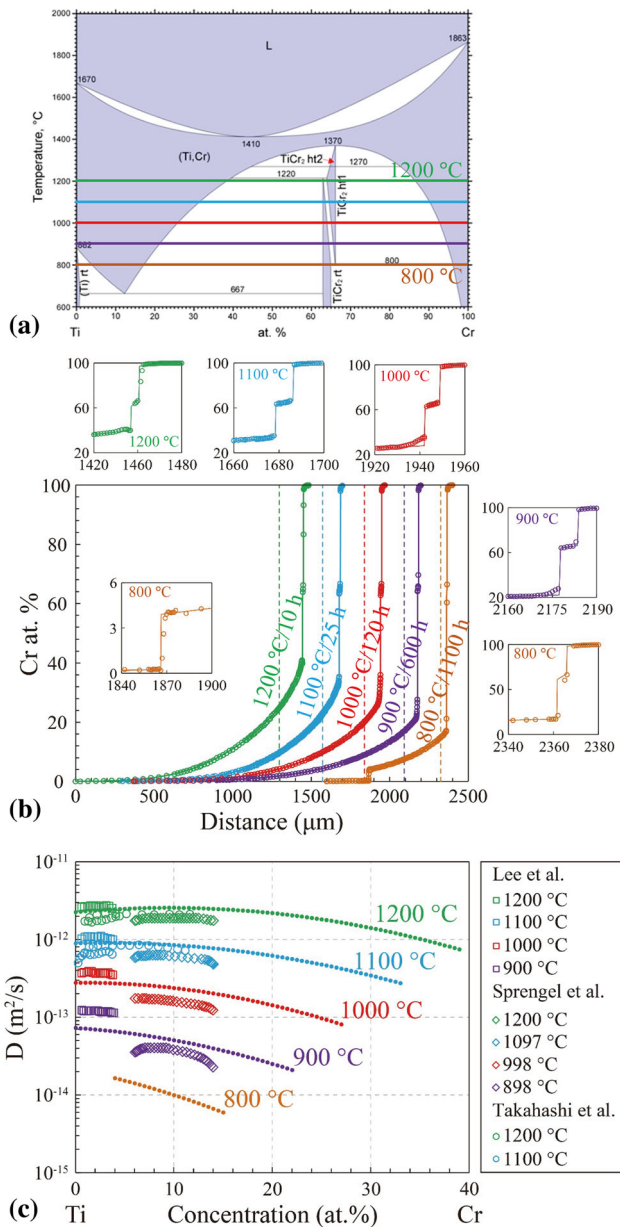


Figure 2 Extracted interdiffusion coefficients of the Ti–Cr binary system at 1200, 1100, 1000, 900, and 800 °C using the forward-simulation method: **a** phase diagram of the Ti–Cr system; **b** experimental and simulated concentration profiles of the Ti–Cr system with the regions near the two-phase interfaces at all annealing temperatures being enlarged and shown in detail as separate insets; and **c** comparison of the interdiffusion coefficients obtained from this study with those reported by Lee et al. [14], Sprengel et al. [15], and Takahashi et al. [16].

1000 °C were extracted first using the composition profiles obtained from the samples annealed at 1000 °C for a total time of 128 h (8 h HIP + 120 h subsequent annealing at 1000 °C), which were used as input to simulate the concentration profiles during

the HIP process at 1000 °C for 8 h. Taking the simulated concentration profile at the end of the HIP process as the initial profile, the diffusion at the other temperatures (i.e., 1200, 1100, 900, and 800 °C) was simulated. Such careful analysis can be readily performed using the forward-simulation method [42, 43] and it would not have been possible using the traditional Boltzmann–Matano analysis.

Since the diffusion coefficients in the hcp phase are usually about two to three orders of magnitude smaller than those in the bcc phase, it is difficult to separate the contribution from the diffusion in the bcc phase during the HIP process before it transforms to the hcp phase at 800 °C. As a result, the extracted diffusion coefficients of the Ti-rich hcp phase in the Ti–Cr, Ti–V, and Ti–Hf systems at 800 °C are deemed to be less accurate and thus not reported in this paper.

The Ti–Cr system

The Ti–Cr binary phase diagram (Fig. 2a) shows four equilibrium solid phases in the temperature range of 800–1200 °C: two solid solutions, α -Ti (hcp) and β -Ti₂Cr (bcc); and two (C15 and C36) TiCr₂ Laves phase intermetallic compounds with narrow composition ranges. The Laves phases have three allotropes designated as α -, β -, and γ -TiCr₂: the low-temperature α -TiCr₂ has a C15 crystal structure which is stable at temperatures below 1220 °C; the intermediate-temperature β -TiCr₂ (C36) is stable between 800 and 1270 °C; and the high-temperature γ -TiCr₂ (C14) is stable at temperatures above 1270 °C. The two-phase region between the α -TiCr₂ and β -TiCr₂ phases seems to be extremely narrow in composition (<1 at.%) and could not be clearly separated from the collected concentration profiles; thus, they were treated as a single-phase for simplicity in the present work for the diffusion coefficient extraction. This assumption has essentially no effect on the evaluated diffusion coefficients of the Ti-rich bcc phases during the forward-simulation process.

The collected experimental concentration profiles at five annealing temperatures together with the corresponding simulated profiles are stacked up and shown together in Fig. 2b. The excellent agreement between the experimental and simulated concentration profiles confirms the reliability of the interdiffusion coefficients extracted using the forward-simulation method.

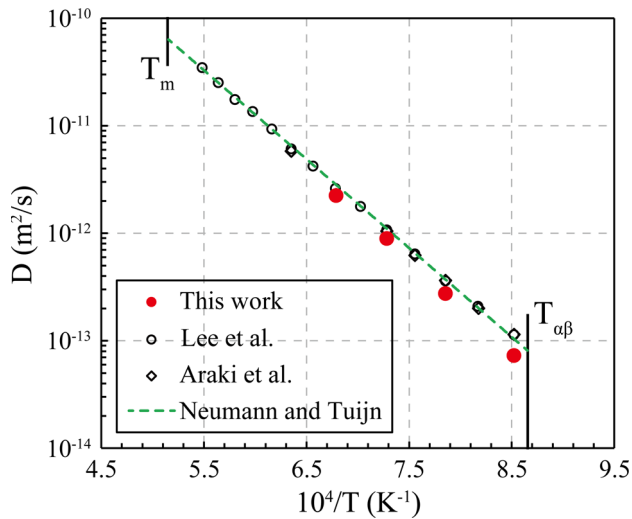


Figure 3 Comparison of the impurity diffusion coefficients of Cr in bcc Ti obtained in this study with the literature data assessed by Neumann and Tuijn [13] as well as the experimental data reported by Lee et al. [14], and Araki et al. [46].

The concentration profiles at both 1000 and 900 °C in Fig. 2b show a sharp increase of the Cr concentration at the edge of the Ti-rich bcc phase (the gradually changing, lower part of Fig. 2b), displaying a sharp upward bend. The compositions at the start of the “bend-over” positions on the 1000 and 900 °C profiles are consistent with the solubility of Cr in the Ti-rich bcc phase as defined by the equilibrium Ti–Cr phase diagram. To the best of our knowledge, such a sharp composition gradient change (the abnormal upward bend) at/near the edge (solubility limit) of a terminal solid solution phase has not been reported before. It is currently postulated that the abnormal upward bend may be the result of a certain phase transformation during the water quench process after the diffusion heat treatment. Since the Cr concentrations in the “bend-over” parts of the 1000 and 900 °C composition profiles are higher than the solubility limits of Cr in the Ti-rich bcc phase at the respective temperatures, it is likely that an interfacial reaction between the Ti-rich bcc phase and the cubic (C15) TiCr_2 Laves phase takes place to form compositions between the two equilibrium phases. This phenomenon will be a subject of future detailed studies. During the forward simulations for diffusion coefficient extraction, the sharp increase (upward bend) in Cr concentration near the edge of the Ti-rich bcc phase is ignored and replaced with an extrapolated line with the same trend as the overall Ti-rich bcc phase composition profile.

A part of the composition profiles for Cr concentrations between the solubility limits in the Ti-rich bcc phase and pure Cr is exceedingly steep as shown in Fig. 2b, resulting in the collection of only a few data points for this wide composition range since the spatial resolution of the EPMA is usually limited to $\sim 1 \mu\text{m}$. Not enough data points can be collected from the sharp composition variation regions to accurately determine the solubility limit of Ti in the Cr-rich bcc phase. The small number of composition points also makes it hard to reliably evaluate the diffusion coefficients in the TiCr_2 and Cr-rich bcc phase. It is thus decided not to report any diffusion coefficient data above the solubility limit of the Ti-rich bcc phase.

The extracted interdiffusion coefficients in the Ti-rich bcc phase at five annealing temperatures are plotted in Fig. 2c in comparison with all the available experimental data from the literature at the temperature range studied [14–16]. It can be seen that our results agree very well with those reported by Takahashi et al. [16] at both 1200 and 1100 °C. The overall agreement with the results of Lee et al. [14] and Sprengel et al. [15] are also reasonable. The results of Lee et al. are slight higher than our values, while the results of Sprengel et al. (whose data were obtained at 2–3 °C lower temperatures) are slightly lower. Our interdiffusion coefficient data cover the entire single-phase compositions of the Ti-rich bcc phase, whereas the literature data are available over only a very limited composition range of 0–15 at.% Cr. In this regards, our more systematic data will contribute significantly to the establishment of reliable diffusion coefficients (mobility) databases for the Ti–Cr system.

The impurity diffusion coefficients of Cr in bcc Ti were obtained from diffusion coefficient extraction using the forward-simulation method [42, 43] based on the Darken’s equation [45] which dictates that the interdiffusion coefficients become the impurity (dilute) diffusion coefficients when the compositions approach the pure elements. The impurity diffusion data of Cr in bcc Ti obtained from the present study are in a very good agreement with those reported by Lee et al. [14], Araki et al. [46], and the assessment by Neumann and Tuijn [13], as shown in Fig. 3. Such a good agreement also gives very high confidence on the extracted interdiffusion coefficients reported in Fig. 2b.

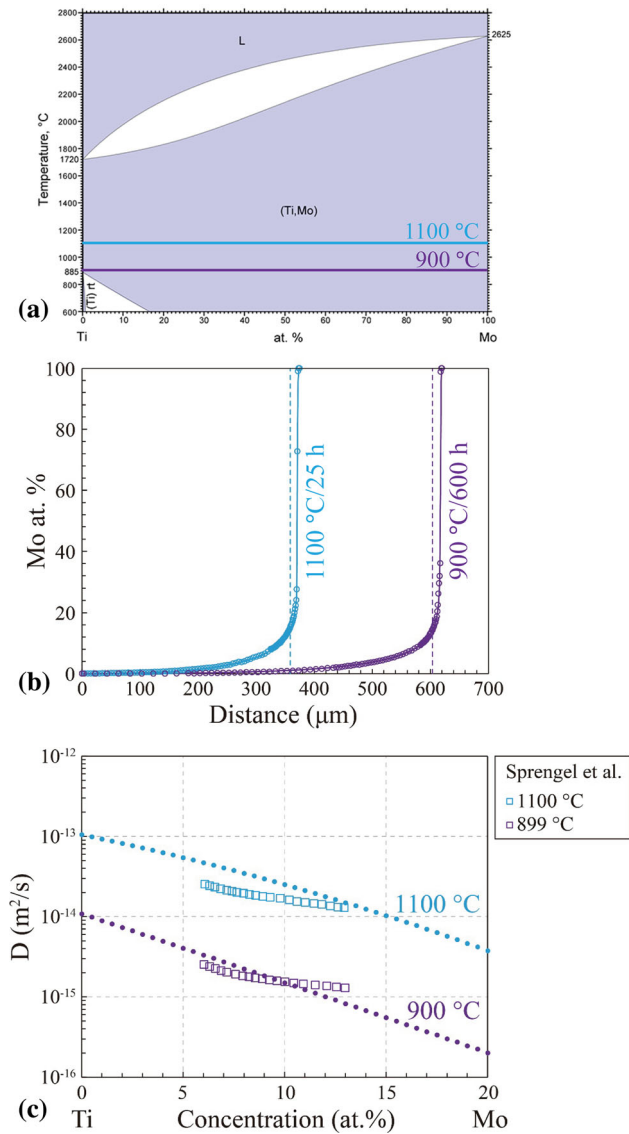


Figure 4 Extracted interdiffusion coefficients of the Ti–Mo binary system at 1100 and 900 °C using the forward-simulation method: **a** phase diagram of the Ti–Mo system; **b** experimental and simulated concentration profiles of the Ti–Mo system; and **c** comparison of the interdiffusion coefficients obtained in this study with those reported by Sprengel et al. [15].

The Ti–Mo system

The Ti–Mo phase diagram in Fig. 4a clearly shows that the bcc Ti and bcc Mo are completely soluble above 882 °C and the Mo solubility in the hcp Ti is very limited, ~1 at.% Mo. The diffusion profiles obtained from the Ti–Mo diffusion couples within the diffusion multiples are extremely asymmetric as shown in Fig. 4b. A very gentle gradient at the Ti-rich side indicates relatively high diffusion coefficients and a

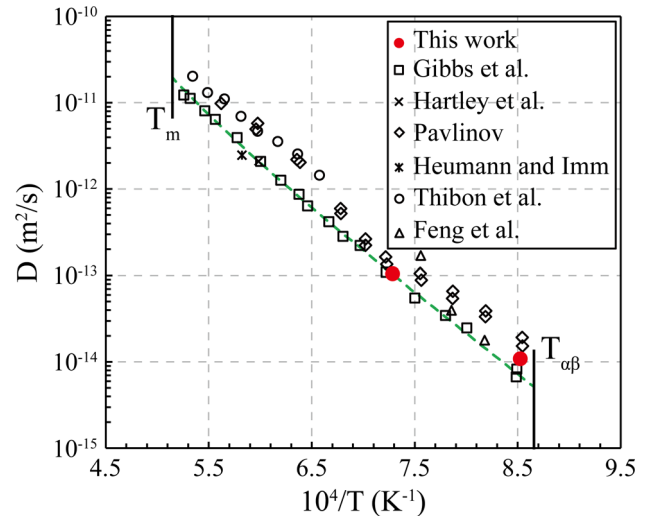


Figure 5 Comparison of the impurity diffusion coefficients of Mo in bcc Ti obtained in this study with the literature data assessed by Neumann and Tuijn [13] as well as the experimental data reported by Gibbs et al. [47], Hartley et al. [17], Pavlinov [48], Heumann and Imm [19], Thibon et al. [22], and Feng et al. [23].

sharp composition gradient at Mo-rich compositions indicates very low diffusion coefficients. For instance, in the composition profile obtained from the sample annealed at 1100 °C for 25 h, the Mo content changes from ~30 to 100 at.% within a 6-μm wide region while the total diffusion distance is ~400 μm, Fig. 4b. The steep concentration gradient is manifested as a visible “interface” in the Mo-rich region within the Ti–Mo diffusion zone as shown in the BSE image in Fig. 1c. The uncertainty is too high for the evaluated interdiffusion coefficients to be reliable for composition regions of extremely sharp gradients, thus we only reported the interdiffusion coefficients from 0 to 20 at.% Mo. In this composition range, the composition profiles can be analyzed very reliably.

Our results in the Ti-rich side agree well with those reported by Sprengel et al. [15] using diffusion couples made up of Ti–5 at.% Mo and Ti–15 at.% Mo alloys as shown in Fig. 4c.

Figure 5 shows the temperature dependence of the impurity diffusivity of Mo in bcc Ti as assessed by Neumann and Tuijn [13] in comparison with the experimental data obtained from this study and those reported in the literature [17, 19, 22, 23, 47, 48]. Our results agree well with Neumann and Tuijn’s collections. The good agreement of impurity diffusion coefficients obtained from the current study lends confidence to our interdiffusion coefficients reported in Fig. 4c.

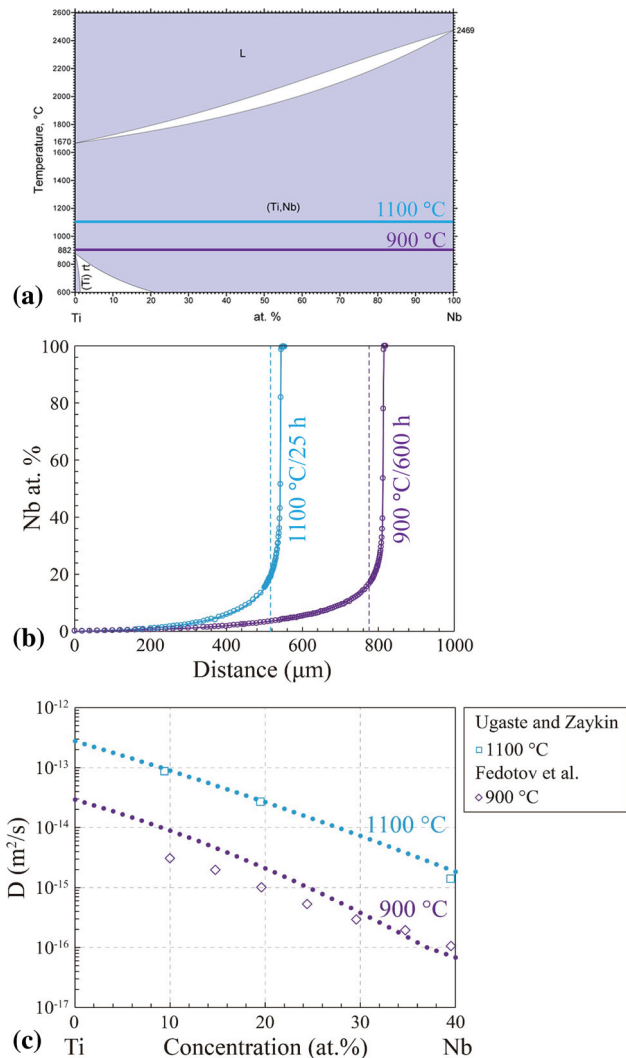


Figure 6 Extracted interdiffusion coefficients of the Ti–Nb binary system at 1100 and 900 °C using the forward-simulation method: **a** phase diagram of the Ti–Nb system; **b** experimental and simulated concentration profiles of the Ti–Nb system; and **c** comparison of the interdiffusion coefficients obtained in this study with those reported by Fedotov et al. [18] and Ugaste and Zaykin [27].

The Ti–Nb system

The phase diagram of the Ti–Nb system is very similar to the Ti–Mo system: the bcc Ti and bcc Nb are completely soluble at both 1100 and 900 °C, Fig. 6a. The concentration profiles obtained from the Ti–Nb diffusion couples are also very asymmetric, as shown in Fig. 6b. Similar to the analysis and discussion of the Ti–Mo system, reliable diffusion coefficients are obtained in the Ti-rich side from 0 up to 40 at.% Nb, Fig. 6c.

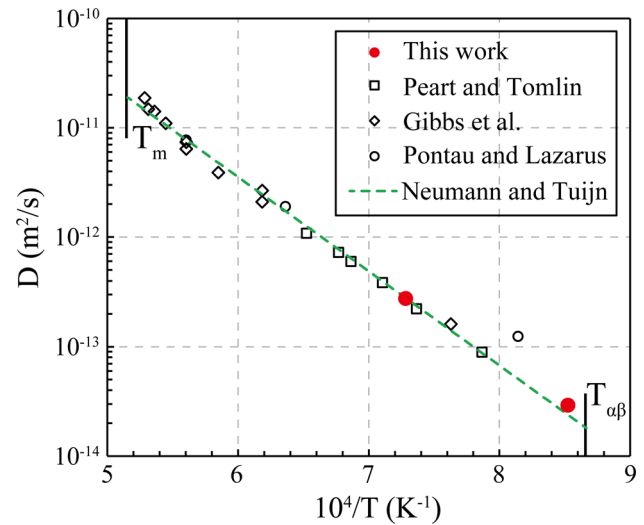


Figure 7 Comparison of the impurity diffusion coefficients of Nb in bcc Ti obtained in this study with the data assessed by Neumann and Tuijn [13] as well as the experimental data reported by Peart and Tomlin [49], Gibbs et al. [47], and Pontau and Lazarus [50].

The impurity diffusion coefficients of Nb in bcc Ti obtained from this study are in excellent agreement with the assessment by Neumann and Tuijn [13] and the results reported in the literature [47, 49, 50], Fig. 7. Such a good agreement with independently measured impurity diffusion coefficients lends credibility to our interdiffusion coefficients reported in Fig. 6c, which also compares the results from this study with the literature data reported by Fedotov et al. [18] and Ugaste and Zaykin [27]. Our results at 1100 °C agree very well with those reported by Ugaste and Zaykin. The results of Fedotov et al. at 900 °C trend towards a much lower impurity diffusion coefficient of Nb in bcc Ti when extrapolated to pure Ti. Since our impurity diffusion coefficient at 900 °C agrees well with the well-assessed values (Fig. 6c), their results are likely less reliable.

The Ti–V system

Similar to the Ti–Mo and Ti–Nb systems, there is a continuous solid solution between the bcc Ti and bcc V above 882 °C as shown in Fig. 8a. The solubility of V in hcp Ti is only ~0.8 at.% at 800 °C according to the phase diagram, while it is measured as 1.1 at.% V in the present study. The bcc (Ti,V) phase in equilibrium with the hcp Ti phase has a composition of ~4.1 at.% Ti at 800 °C according to the phase diagram, while the measured value is ~5.1 at.% Ti from

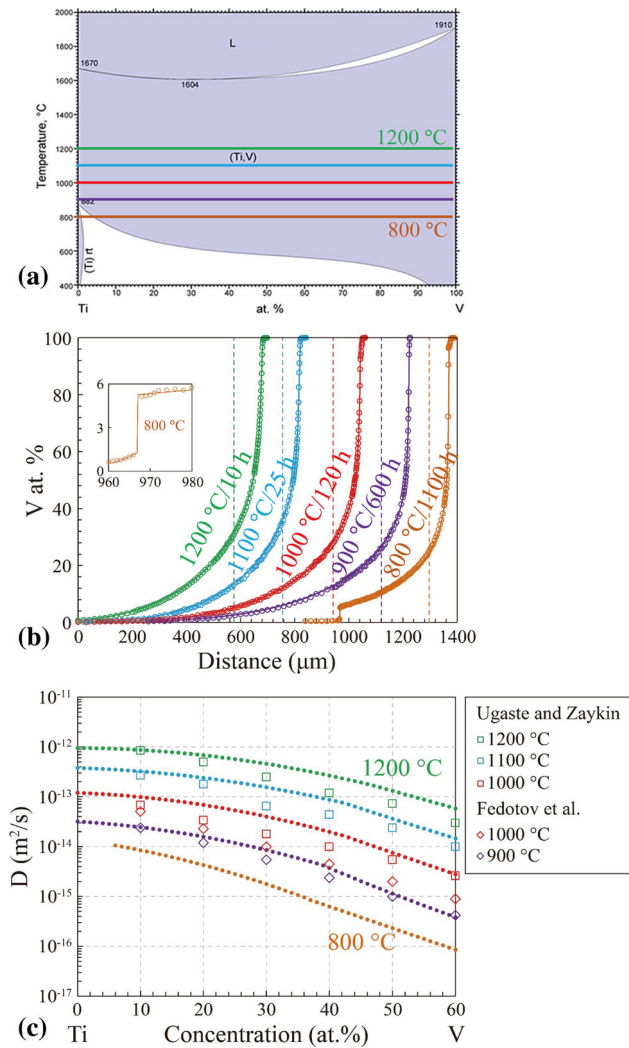


Figure 8 Extracted interdiffusion coefficients of the Ti–V binary system at 1200, 1100, 1000, 900, and 800 °C using the forward-simulation method: **a** phase diagram of the Ti–V system; **b** experimental and simulated concentration profiles of the Ti–V system with the region near the two-phase interface at 800 °C being enlarged and shown in detail as a separate inset; and **c** comparison of the interdiffusion coefficients obtained in this study with those reported by Fedotov et al. [18] and Ugaste and Zaykin [27].

the 800 °C diffusion profile of this study, Fig. 8b. The diffusion profiles obtained from the Ti–V diffusion couples are also extremely asymmetric as those of the Ti–Mo and Ti–Nb systems, as shown in Fig. 8b. Reliable results in the Ti-rich part from 0 up to 60 at.% V are reported in this study.

The interdiffusion coefficients extracted using the forward-simulation method are summarized in Fig. 8c and compared with literature data from

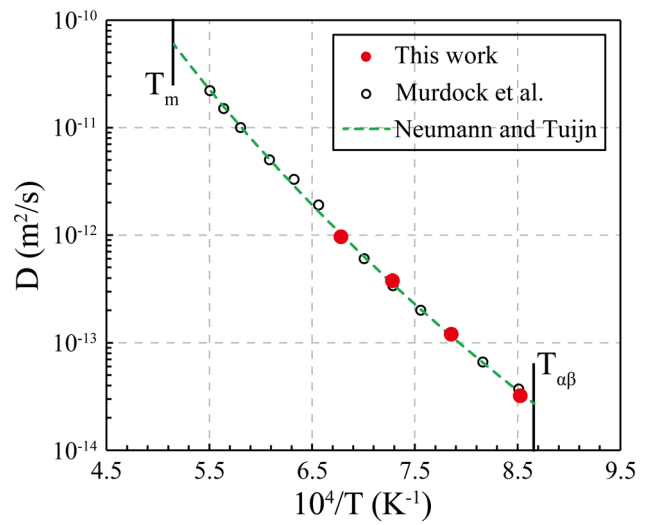


Figure 9 Comparison of the impurity diffusion coefficients of V in bcc Ti obtained in this study with the data assessed by Neumann and Tuijn [13] as well as the experimental data reported by Murdock et al. [51].

Fedotov et al. [18] and Ugaste and Zaykin [27]. Our results at 900 °C agree well with the results of Fedotov et al., while our results at 1000–1200 °C are slightly higher than those of Fedotov et al. and Ugaste and Zaykin.

Figure 9 shows an excellent agreement between the impurity diffusion coefficients of V in bcc Ti obtained from this study with the assessment by Neumann and Tuijn [13] and the results reported by Murdock et al. [51], again lending more credibility to our interdiffusion coefficient data shown in Fig. 8c.

The Ti–Hf system

Both Ti and Hf exhibit the bcc phase at high temperatures and the hcp phase at low temperatures, and they form continuous bcc and hcp solid solutions with a narrow two-phase region in between, as shown in Fig. 10a. From 900 to 1200 °C, there are the Ti-rich bcc solid solution and the Hf-rich hcp solid solution. All the concentration profiles collected using EPMA from the Ti–Hf diffusion couples inside the diffusion multiples annealed at 900–1200 °C are summarized in Fig. 10b. Very steep gradients of compositions were observed in the Hf-rich hcp phase region, indicating very low diffusion coefficients. As mentioned in the discussions of other binary systems, diffusion coefficients extracted from such steep gradients are not very reliable and thus are not reported here.

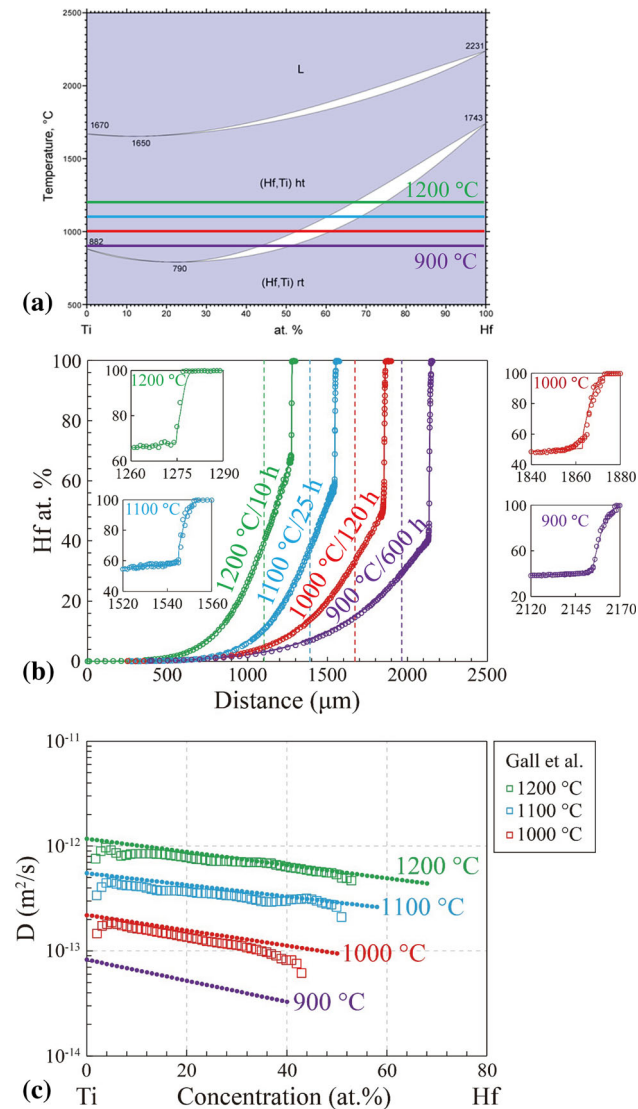


Figure 10 Extracted interdiffusion coefficients of the Ti–Hf binary system at 1200, 1100, 1000, and 900 °C using the forward-simulation method: **a** phase diagram of the Ti–Hf system; **b** experimental and simulated concentration profiles of the Ti–Hf system with the regions near the two-phase interfaces at 900–1200 °C being enlarged and shown in detail as separate insets; and **c** comparison of the interdiffusion coefficients obtained in this study with those reported by Gall et al. [28].

Similar to the concentration profiles of the Ti–Cr system, a sharp increase of the Hf concentration at the edge (solubility limit) of the bcc phase was observed at both the 1000 and 900 °C concentration profiles, Fig. 10b. The same approach employed for the Ti–Cr system is applied to the Ti–Hf binary concentration profile analysis.

The interdiffusion coefficients extracted using the forward-simulation method are summarized in

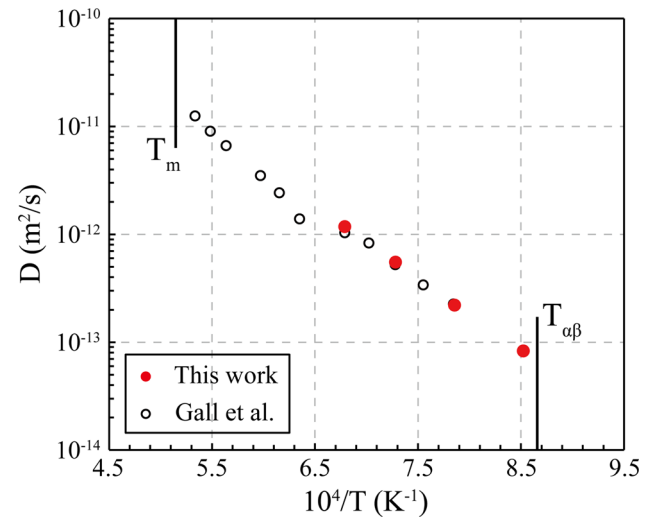


Figure 11 Comparison of the impurity diffusion coefficients of Hf in bcc Ti obtained in this study with those reported by Gall et al. [28].

Fig. 10c and compared to the results of Gall et al. [28], showing a very good agreement. The impurity diffusion coefficients obtained from the current study are also in excellent agreement with those of Gall et al., Fig. 11.

The Ti–Zr system

Similar to the Ti–Hf system, the Ti–Zr phase diagram shows complete solubility in both the bcc and hcp phases at high and low temperatures, respectively, as shown in Fig. 12a. The high-temperature bcc phase is a continuous solid solution at both 1100 and 900 °C. The obtained composition profiles at both temperatures are very wide without very sharp compositional changes as shown in Fig. 12b, thus the diffusion coefficients can be obtained for the entire composition range. An abnormal increase of the Zr content close to pure Zr was observed in the 900 °C composition profile, and the exact reason is currently unknown. An extrapolated composition line over 98 at.% Zr with the same trend as that in the bcc phase was used for the forward simulations to obtain the diffusion coefficients.

The interdiffusion coefficients extracted using the forward-simulation method are summarized in Fig. 12c and compared with the results reported in the literature [30–32], showing a good overall agreement. Figure 13 compares the impurity diffusion coefficients of Ti in bcc Zr and Zr in bcc Ti obtained from this study with the assessment by Neumann and Tuijn [13]

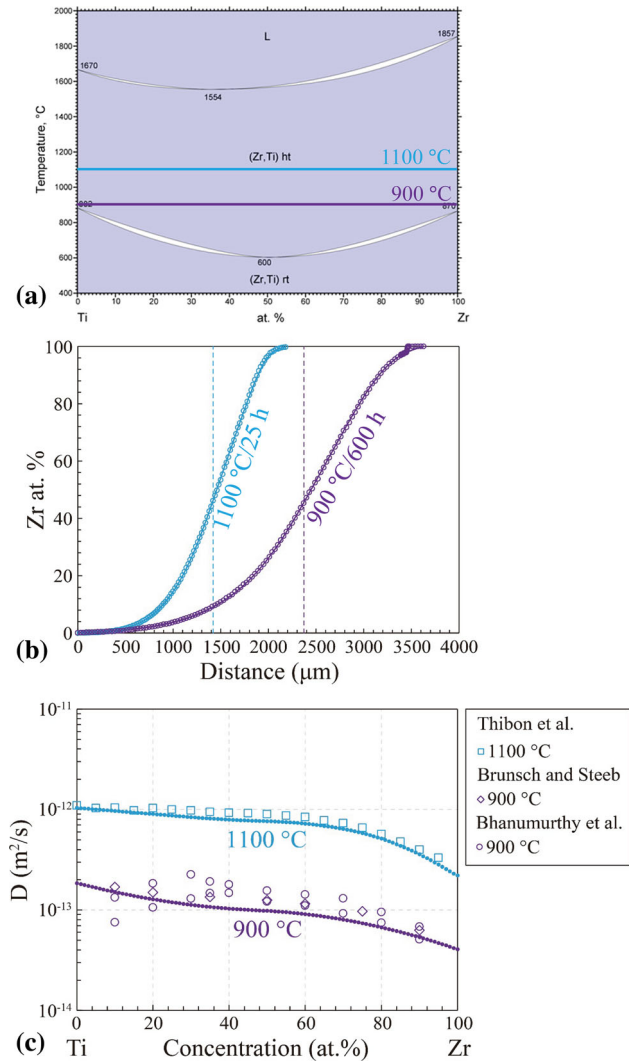


Figure 12 Extracted interdiffusion coefficients of the Ti–Zr binary system at 1100 and 900 °C using the forward-simulation method: **a** phase diagram of the Ti–Zr system; **b** experimental and simulated concentration profiles of the Ti–Zr system; and **c** comparison of the interdiffusion coefficients obtained in this study with those reported by Brunsch and Steeb [30], Bhanumurthy et al. [31], and Thibon et al. [32].

and experimental data reported in the literature [29, 31, 32, 48, 52]. Our results agree well with most of the literature data except for the results from Raghunathan et al. [29] and Bhanumurthy et al. [31]. The impurity diffusion coefficients of Zr in bcc Ti from Raghunathan et al. are only extrapolated from the interdiffusion coefficients and the values are not consistent with the other datasets. The impurity diffusion data from Bhanumurthy et al. [31] are calculated using both the Boltzmann–Matano method and the Hall method. The values extrapolated from the Boltzmann–

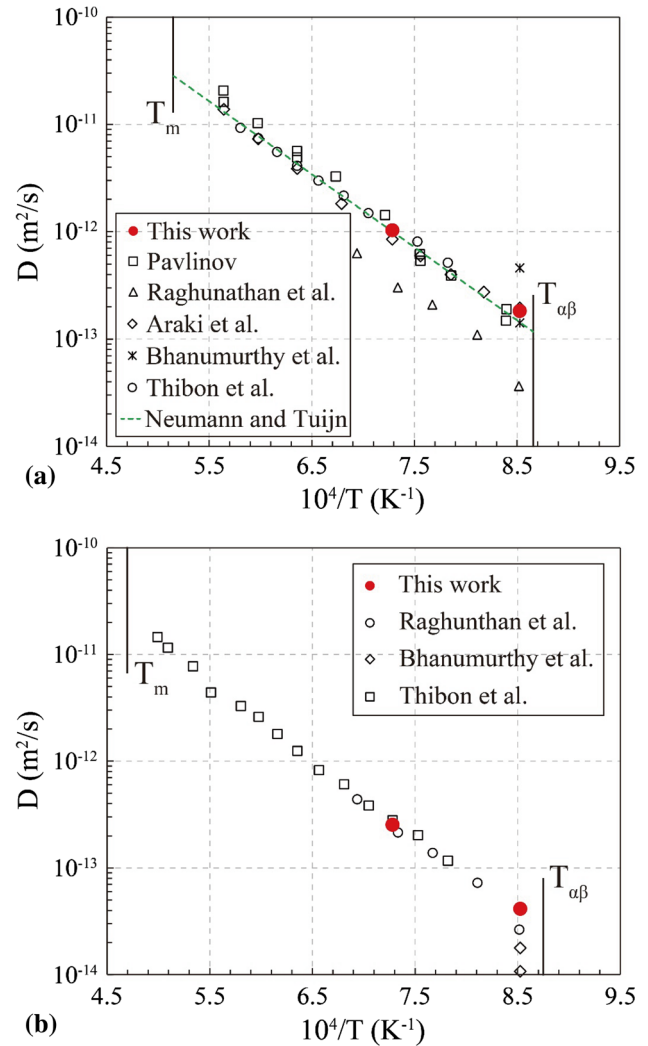


Figure 13 Comparison of the impurity diffusion coefficients obtained in this study with the data assessed by Neumann and Tuijn [13] as well as the experimental data reported by Pavlinov [48], Raghunathan et al. [29], Araki et al. [52], Bhanumurthy et al. [31], and Thibon et al. [32]: **a** Zr in bcc Ti and **b** Ti in bcc Zr.

Matano method show a satisfactory agreement with the assessment of Neumann and Tuijn, while the Hall method gives less satisfactory results. A recent work by Ahmed et al. [53] conclusively shows that the Hall method can only give a good accuracy for composition-independent interdiffusion coefficients. Thus, the impurity diffusion coefficients obtained using the Hall method by Bhanumurthy et al. are less reliable when the interdiffusion coefficients change significantly with composition.

One can clearly see that the combination of high-throughput diffusion multiples with the forward-simulation method can provide much-needed

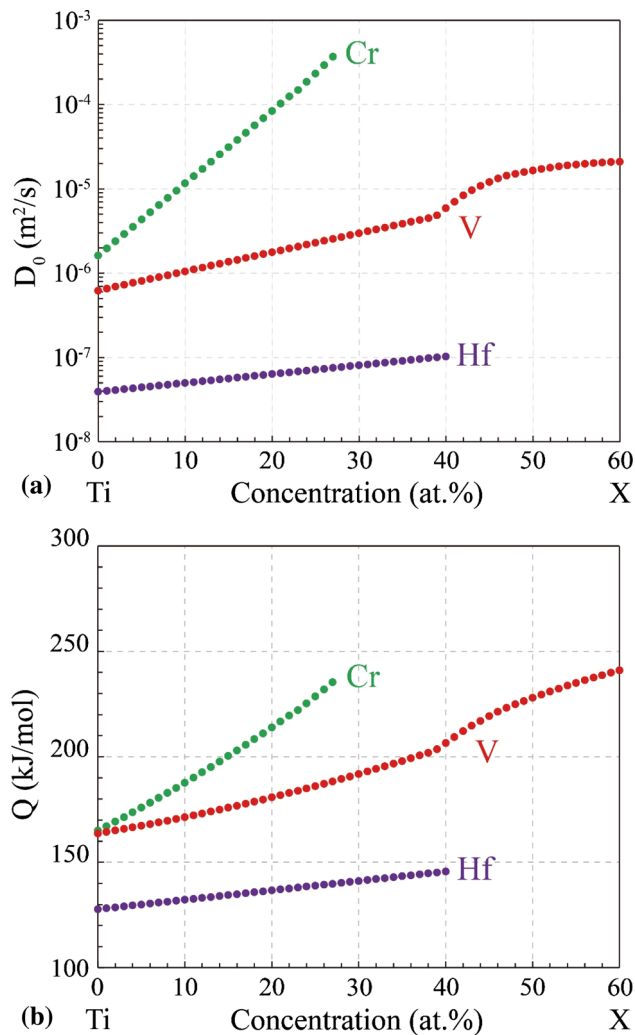


Figure 14 The evaluated pre-exponential factor D_0 (a) and activation energy Q (b) as a function of Cr, Hf, and V concentrations (all in at.%).

diffusion coefficients, especially impurity diffusion coefficients which are usually measured by time-consuming tracer experiments. The present work systematically measured the diffusion coefficients in the bcc phase of the Ti–Cr, Ti–Hf, Ti–Mo, Ti–Nb, Ti–V, and Ti–Zr systems, which are essential for the establishment of reliable diffusion (mobility) databases. The obtained composition-dependent diffusion coefficients in the temperature range of 900–1200 °C allow us to perform Arrhenius analysis in order to evaluate the pre-exponential factor D_0 and the activation energy Q as a function of composition. The values of D_0 and Q as a function of Cr, Hf, and V concentrations (all in at.%) are plotted in Fig. 14. As can be seen, both the D_0 and Q increase as Cr, Hf, and V concentrations increase.

Summary

A set of five identical Ti–TiAl–Cr–Hf–Mo–Nb–V–Zr diffusion multiples were fabricated and annealed at 1200, 1100, 1000, 900, and 800 °C for 10, 25, 120, 600, and 1100 h, respectively. EPMA line scans were performed parallel to the diffusion direction to obtain the concentration profiles from the Ti–X (X = Cr, Hf, Mo, Nb, V, Zr) diffusion couples inside the five diffusion multiples. The composition-dependent interdiffusion coefficients were extracted from the collected diffusion profiles using the forward-simulation method [42, 43]. Very large amounts of systematic diffusion coefficient data on the Ti-rich bcc phase at several temperatures are obtained and compared with prior literature data.

Impurity diffusion coefficients were obtained from the binary composition profiles using the forward-simulation method on the basis of Darken’s equation. Twenty (20) impurity diffusion coefficient values of X (X = Cr, Hf, Mo, Nb, V, Zr) in bcc Ti and Ti in bcc Zr agree well with the independently measured literature data (some of them from tracer experiments)—it would take tremendous amount of time to perform 20 tracer measurements. The excellent agreement of our impurity diffusion coefficients with independently measured values in the literature also lends credibility to the extracted interdiffusion coefficients in the Ti-rich bcc phase in the current study, as well as the general methodology employed in this study. The large amount of reliable diffusion coefficients obtained from this study will be valuable input for the establishment of reliable diffusion (mobility) databases for the kinetic modeling of Ti alloys.

The present study only obtained reliable diffusion coefficient data in the Ti-rich part of the Ti–X (X = Cr, Mo, Nb, V, Hf) systems. More careful investigations using semi-infinite diffusion couples made up of Ti–X alloys and pure X’s are recommended with longer annealing durations to study the diffusion behaviors in the Ti-lean regions of the binary systems.

Acknowledgements

Financial supports by grants from the Major State Basic Research Development Program of China (No. 2014CB6644002 and No. 2012CB619501) and the National Key Research Development Plan (No.

2016YFB0701301) are gratefully acknowledged. The work is also partially supported by the Project of Innovation-driven Plan in Central South University (No. 2015CX004) and the outstanding graduate project of Advanced Non-ferrous Metal Structural Materials and Manufacturing Collaborative Innovation Center.

References

- [1] Leyens C, Peters M (2003) Titanium and titanium alloys. Wiley-VCH, Weinheim
- [2] Lütjering G, Williams JC (2003) Titanium, 2nd edn. Springer, New York
- [3] Niinomi M (2002) Recent metallic materials for biomedical applications. *Metall Mater Trans A* 33:477–486
- [4] Geetha M, Singh AK, Asokamani R, Gogia AK (2009) Ti based biomaterials, the ultimate choice for orthopaedic implants—a review. *Prog Mater Sci* 54:397–425
- [5] Niinomi M, Kuroda D, K-i Fukunaga, Morinaga M, Kato Y, Yashiro T, Suzuki A (1999) Corrosion wear fracture of new β type biomedical titanium alloys. *Mater Sci Eng A* 263:193–199
- [6] Eisenbarth E, Velten D, Müller M, Thull R, Breme J (2004) Biocompatibility of β -stabilizing elements of titanium alloys. *Biomaterials* 25:5705–5713
- [7] Song Y, Xu DS, Yang R, Li D, Wu WT, Guo ZX (1999) Theoretical study of the effects of alloying elements on the strength and modulus of β -type bio-titanium alloys. *Mater Sci Eng A* 260:269–274
- [8] Wang BL, Li L, Zheng YF (2010) In vitro cytotoxicity and hemocompatibility studies of Ti–Nb, Ti–Nb–Zr and Ti–Nb–Hf biomedical shape memory alloys. *Biomed Mater* 5:044102
- [9] González M, Peña J, Manero JM, Arciniegas M, Gil FJ (2009) Design and characterization of new Ti–Nb–Hf alloys. *J Mater Eng Perform* 18:490–495
- [10] González M, Gil FJ, Manero JM, Peña J (2011) Characterization of two Ti–Nb–Hf–Zr alloys under different cold rolling conditions. *J Mater Eng Perform* 20:653–657
- [11] González M, Salvagni E, Rodríguez-Cabello JC, Rupérez E, Gil FJ, Peña J, Manero JM (2013) A low elastic modulus Ti–Nb–Hf alloy bioactivated with an elastin-like protein-based polymer enhances osteoblast cell adhesion and spreading. *J Biomed Mater Res A* 101A:819–826
- [12] González M, Peña J, Gil FJ, Manero JM (2014) Low modulus Ti–Nb–Hf alloy for biomedical applications. *Mater Sci Eng C* 42:691–695
- [13] Neumann G, Tuijn C (2011) Self-diffusion and impurity diffusion in pure metals: handbook of experimental data. Elsevier, Oxford
- [14] Lee S-Y, Iijima Y, Hirano K-I (1991) Diffusion of chromium and palladium in β -titanium. *Mater Trans JIM* 32:451–456
- [15] Sprengel W, Yamada T, Nakajima H (1997) Interdiffusion in binary β -titanium alloys. *Defect Diff Forum* 143–147:431–436
- [16] Takahashi T, Matsuda N, Kubo S, Hino T, Komatsu M, Hisayuki K (2004) Interdiffusion in the β solid solution of Ti–Al–Cr system. *J Jpn Inst Light Met* 54:280–286
- [17] Hartley CS, Steedly JE, Parsons LD (1965) Binary interdiffusion in body-centered cubic transition metal systems. In: Wheeler JA, Winslow FR (eds) *Diffusion in body-centered cubic metals*. American Society for Metals, Metals Park, pp 51–75
- [18] Fedotov SG, Chudinov MG, Konstantinov KM (1969) Mutual diffusion in the systems Ti–V, Ti–Nb, Ti–Ta, and Ti–Mo. *Fiz Met Metalloved* 27:111–114
- [19] Heumann T, Imm R (1978) Study of the Kirkendall effect in bcc titanium–molybdenum alloys. *Forschungsberichte des Landes Nordrhein-Westfalen* 2781:5–25
- [20] Majima K, Isomoto T (1982) The sintering characteristics and diffusion processes of the titanium–molybdenum binary system. *J Jpn Soc Powder Metall* 29:280–285
- [21] Kale G, Patil R (1994) Chemical diffusion in titanium–molybdenum system. *Mater Trans JIM* 35:439–444
- [22] Thibon I, Ansel D, Boliveau M (1998) Interdiffusion in the β Mo–Ti solid solution at high temperatures. *Z Metallkd* 89:187–191
- [23] Feng L, Li J, Huang L, Chang H, Cui Y, Zhou L (2009) Interdiffusion behavior of Ti–Mo binary system in β phase. *Chin J Nonferrous Met* 19:1766–1771
- [24] Roux F, Vignes A (1970) Diffusion dans les systèmes Ti–Nb, Zr–Nb, V–Nb, Mo–Nb, W–Nb. *Rev Phys Appl* 5:393–405
- [25] Polyanskii VM, Podgorskii BN, Makarovets OD (1971) Diffusion processe in the Ti–Nb system. *Svar Proizvod* 3:9–10
- [26] Gryzunov VI, Aitbaev BK, Omasheva G, Fryzunova TI (1993) Interdiffusion in the titanium–niobium system. *Seriya Khim* 6:29–33
- [27] Ugaste YE, Zajkin YA (1975) Investigation of mutual diffusion in titanium–vanadium and titanium–niobium systems. *Fiz Met Metalloved* 40:567–575
- [28] Le Gall G, Ansel D, Debuigne J (1987) Interdiffusion in the body cubic centered β -phase of titanium–hafnium alloys. *Acta Metall* 35:2297–2305
- [29] Raghunathan VS, Tiwari GP, Sharma BD (1972) Chemical diffusion in the β phase of the Zr–Ti alloy system. *Metall Trans* 3:783–788
- [30] Brunsch A, Steeb S (1974) Diffusion investigation in the Ti–Zr system by means of a microprobe. *Z Naturforsch A* 29:1319–1324

- [31] Bhanumurthy K, Laik A, Kale G (2008) Novel method of evaluation of diffusion coefficients in Ti–Zr system. *Defect Diff Forum* 279:53–62
- [32] Thibon I, Ansel D, Gloriant T (2009) Interdiffusion in β -Ti–Zr binary alloys. *J Alloys Comp* 470:127–133
- [33] Boltzmann L (1894) Zur integration der diffusionsgleichung bei variabeln diffusionskoeffizienten. *Ann Phys* 289:959–964
- [34] Matano C (1933) On the relation between the diffusion-coefficients and concentrations of solid metals (the nickel–copper system). *Jpn J Phys* 8:109–113
- [35] den Broeder FJA (1969) A general simplification and improvement of the matano-boltzmann method in the determination of the interdiffusion coefficients in binary systems. *Scr Metall* 3:321–325
- [36] Hall LD (1953) An analytical method of calculating variable diffusion coefficients. *J Chem Phys* 21:87–89
- [37] Zhao J-C (2001) A combinatorial approach for structural materials. *Adv Eng Mater* 3:143–147
- [38] Zhao J-C, Jackson MR, Peluso LA, Brewer LN (2002) A diffusion multiple approach for the accelerated design of structural materials. *MRS Bull* 27:324–329
- [39] Zhao J-C (2004) Reliability of the diffusion-multiple approach for phase diagram mapping. *J Mater Sci* 39:3913–3925. doi:10.1023/B:JMISC.0000031472.25241.c5
- [40] Zhao J-C (2007) *Methods for phase diagram determination*. Elsevier, Amsterdam, pp 246–272
- [41] van Loo FJJ (1990) Multiphase diffusion in binary and ternary solid-state systems. *Prog Solid State Chem* 20:47–99
- [42] Zhang Q, Zhao J-C (2013) Extracting interdiffusion coefficients from binary diffusion couples using traditional methods and a forward-simulation method. *Intermetallics* 34:132–141
- [43] Zhang Q, Zhao J-C (2014) Impurity and interdiffusion coefficients of the Cr–X (X = Co, Fe, Mo, Nb, Ni, Pd, Pt, Ta) binary systems. *J Alloys Compd* 604:142–150
- [44] ASM Alloy Phase Diagram Center. <http://www1.asminternational.org/asmenterprise/apd/>. Accessed Dec 2014
- [45] Darken LS (1948) Diffusion, mobility and their interrelation through free energy in binary metallic systems. *Trans AIME* 175:184–201
- [46] Araki H, Yamane T, Nakatuka T, Minamino Y (2006) Diffusion of chromium in β -Ti under high pressure. *Z Metallkd* 97:22–27
- [47] Gibbs GB, Graham D, Tomlin DH (1963) Diffusion in titanium and titanium–niobium alloys. *Philos Mag* 8:1269–1282
- [48] Pavlinov LB (1967) Diffusion of metal impurities in zirconium and titanium (Heterodiffusion of metallic impurities in body centered phases of doped zirconium and titanium, determining diffusion coefficients via radioactive isotopes). *Phys Met Metall* 24:70–74
- [49] Peart RF, Tomlin DH (1962) Diffusion of solute elements in beta-titanium. *Acta Metall* 10:123–134
- [50] Pontau AE, Lazarus D (1979) Diffusion of titanium and niobium in bcc Ti–Nb alloys. *Phys Rev B* 19:4027–4037
- [51] Murdock JF, Lundy TS, Stansbury EE (1964) Diffusion of Ti^{44} and V^{48} in titanium. *Acta Metall* 12:1033–1039
- [52] Araki H, Minamino Y, Yamane T, Nakatsuka T, Miyamoto Y (1996) Pressure dependence of anomalous diffusion of zirconium in β -titanium. *Metall Trans A* 27:1807–1814
- [53] Ahmed T, Belova IV, Evteev AV, Levchenoko EV, Murch GE (2015) Comparison of the Sauer-Freise and Hall methods for obtaining interdiffusion coefficients in binary alloys. *J Phase Equilib Diffu* 36:366–374